

AD-A088 409

# TECHNICAL LIBRARY

AD

AD-E400 457

SPECIAL PUBLICATION ARSCD-SP-80001

## A COMPARISON OF RESIDUAL STRESS MEASURING TECHNIQUES: THEIR STRENGTHS AND WEAKNESSES

FRED M. WITT

FEE M. LEE

WALTER M. RIDER

AUGUST 1980



**US ARMY ARMAMENT RESEARCH AND DEVELOPMENT COMMAND**  
**FIRE CONTROL AND SMALL CALIBER**  
**WEAPON SYSTEMS LABORATORY**  
**DOVER, NEW JERSEY**

APPROVED FOR PUBLIC RELEASE; DISTRIBUTION UNLIMITED.

The views, opinions, and/or findings contained in this report are those of the author(s) and should not be construed as an official Department of the Army position, policy or decision, unless so designated by other documentation.

Destroy this report when no longer needed. Do not return it to the originator.

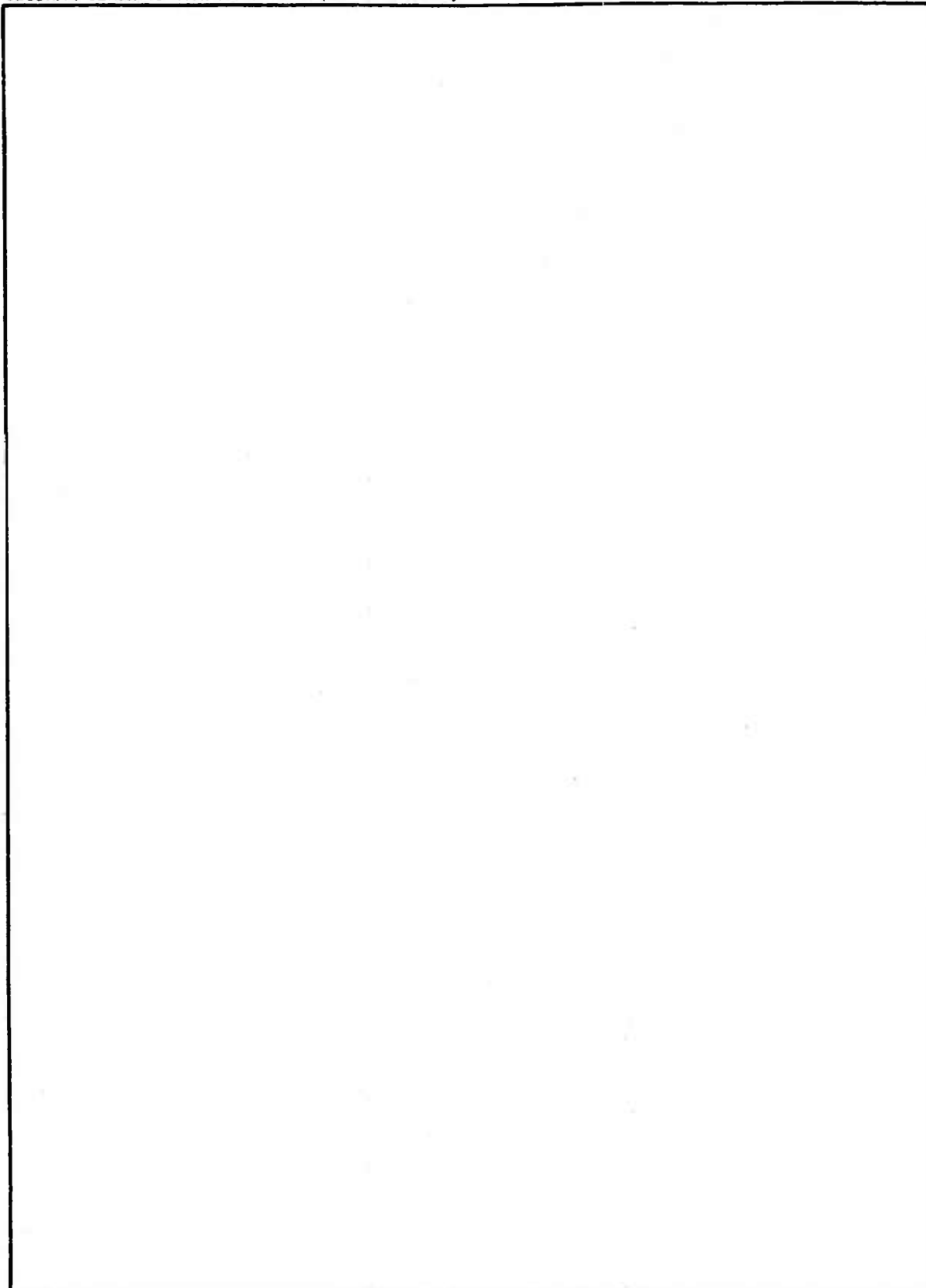
The citation in this report of the names of commercial firms or commercially available products or services does not constitute official endorsement or approval of such commercial firms, products, or services by the United States Government.

UNCLASSIFIED

SECURITY CLASSIFICATION OF THIS PAGE (When Data Entered)

REPORT DOCUMENTATION PAGE		READ INSTRUCTIONS BEFORE COMPLETING FORM
1. REPORT NUMBER Special Publication ARLCD-SP-80001	2. GOVT ACCESSION NO.	3. RECIPIENT'S CATALOG NUMBER
4. TITLE (and Subtitle) A Comparison of Residual Stress Measuring Techniques: Their Strengths and Weaknesses		5. TYPE OF REPORT & PERIOD COVERED
		6. PERFORMING ORG. REPORT NUMBER
7. AUTHOR(s) Fred Witt Fee M. Lee Walter M. Rider		8. CONTRACT OR GRANT NUMBER(s)
9. PERFORMING ORGANIZATION NAME AND ADDRESS ARRADCOM, FC&SCWSL M&MT Div. (DRDAR-SCM-P) Dover, NJ 07801		10. PROGRAM ELEMENT, PROJECT, TASK AREA & WORK UNIT NUMBERS AMCMS Code 6111 .01 .91A DA Project 11161101A91A
11. CONTROLLING OFFICE NAME AND ADDRESS ARRADCOM, TSD STINFO Div. (DRDAR-TSS) Dover, NJ 07801		12. REPORT DATE Aug 1980
		13. NUMBER OF PAGES 31
14. MONITORING AGENCY NAME & ADDRESS (If different from Controlling Office)		15. SECURITY CLASS. (of this report)  UNCLASSIFIED
		15e. DECLASSIFICATION/DOWNGRADING SCHEDULE
16. DISTRIBUTION STATEMENT (of this Report)  Approved for public release; distribution unlimited.		
17. DISTRIBUTION STATEMENT (of the abstract entered in Block 20, if different from Report)		
18. SUPPLEMENTARY NOTES		
19. KEY WORDS (Continue on reverse side if necessary and identify by block number)		
Residual stress	Electric discharge machining	Line shift
Strain gage methods	Abrasive jet machining	Subgrain interior
X-ray methods	Stress concentration factor	
Rotating cutters	Point gage	
20. ABSTRACT (Continue on reverse side if necessary and identify by block number)		
<p>Ongoing in-house work on the measurement of residual stress in Army Materiel by both X-ray and strain gage mechanical relaxation methods is presented and compared. The X-ray portion includes problems associated with the calculation of stresses in highly textured samples while the strain gage portion describes effects produced by various mechanical methods to partially relieve the strain fields sensed by the active gage elements. Comparisons are also made of the errors introduced by considering the active element in the strain gage rosette as a point gage instead of one with finite length.</p>		

SECURITY CLASSIFICATION OF THIS PAGE(When Data Entered)



SECURITY CLASSIFICATION OF THIS PAGE(When Data Entered)

## TABLE OF CONTENTS

	<u>Page No.</u>
Introduction	1
Circumferential Stress by Longitudinal Slitting	1
Blind Hole Drilling Methods	3
Hole Forming Methods	4
Abrasive Jet Method	7
Indeterminacy of Beta	9
Effect of the Central Hole on the Measured Stress	9
X-ray Measurement of Stress	11
Summary	14
References	15
Distribution List	19

## FIGURES

1	Crampton's method for computing the circumferential stress in thin wall tubes	2
2	Relationship between the linear strain gage elements and the principal directions	4
3	Strain effects caused by various hole producing methods	5
4	Experimental setup for abrasive jet machining	7
5	Effect of the stress concentration factor on the state of stress in a uniaxially stressed plate	10
6	Interplanar spacing plot for different residual stress states	12

	<u>Page No.</u>
7 Lattice and total stress-strain curve	13

TABLE

Effect of using point gage versus finite length gage equations in the computation of residual stress	8
---	---

## INTRODUCTION

Residual stresses are those stresses which reside in the bulk of a material when the external forces acting on it are removed. One customarily excludes external forces such as gravity or thermal gradients. Since the body under consideration is in equilibrium, the resultant force equals zero. This report describes methods used to circumvent some pitfalls encountered when standard X-ray and strain gage methods are indiscriminately used to measure residual stress.

When the residual stresses are long range in nature, that is, are reasonably constant in magnitude, sign, and direction, and extend over distances comparable to many grain diameters, they are termed macrostresses. As such they are easily measured by mechanical methods employing dissection, layer removal, and careful hole-drilling procedures. Stresses of this type produce an X-ray line shift when the sample is rotated in an X-ray beam. On the other hand, when the residual stresses are short range in nature, and vary appreciably over distances comparable to the grain diameter, they are called microstresses. These cannot be detected by mechanical dissection methods and may or may not produce an X-ray line shift, depending on the distances over which the microstresses exert their influence. For example, when the stress acting distance is approximately a micron, X-ray line broadening and line shifts are observed. As this distance shrinks to approximately 1000 Å or less, X-ray line broadening persists, but line shifts are not observed.

Furthermore, when the actual deformation mode produces extensive movement of material in a given direction, complications arise which prohibit the use of X-ray methods and computational formulas. In other words, the standard X-ray analysis can produce erroneous results for cases where the specimens have been extensively rolled, drawn, stretched, compressed, or bent. The standard X-ray methods do, however, produce reliable answers when the measurement is made on surfaces which have been machined, ground, or peened (ref 1). Here the mass movement is not predominantly unidirectional. A relatively unknown, but straightforward way, does exist, however, to correct for the deficiencies of the standard X-ray method when extensive amounts of uniaxial plastic metal flow has occurred. The method, reported by Marion and Cohen (ref 2), will be described in a later section. Some discussion will now be given concerning several problems the authors have encountered, using some of the "handbook" approaches to determine the stress state of various specimens.

## CIRCUMFERENTIAL STRESS BY LONGITUDINAL SLITTING

The stress condition of thin wall tubes is sometimes assessed by

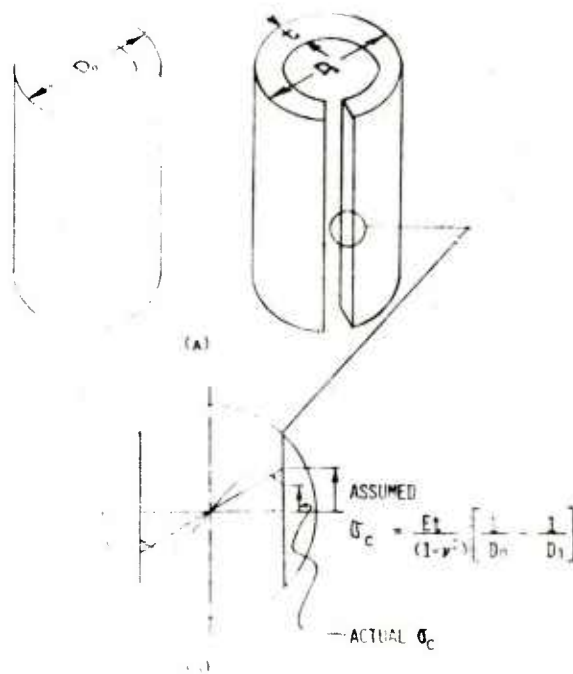


Figure 1. Crampton's method for computing the circumferential stress in thin wall tubes.

Crampton's method (figure 1). Here one slits a tube its entire length along one element and makes use of the beam formula to compute the maximum circumferential stress. The method assumes that a condition of plane strain exists. In other words, the strain and curvature change in the longitudinal direction are zero. According to Crampton, the circumferential stress on the outer fibers is given by,

$$\sigma_c = \frac{Et}{(1-\nu^2)} \left[ \frac{1}{D_0} - \frac{1}{D_1} \right] \quad (1)$$

Where E is Young's modulus, t is the wall thickness,  $\nu$  is Poisson's ratio,  $D_0$  is the mean diameter before slitting, and  $D_1$  is the mean diameter after slitting. It can be seen from equation 1 that a tensile stress on the outside surface of the tube causes  $D_1$  to be larger than  $D_0$ ; while a compressive stress causes  $D_1$  to be smaller than  $D_0$ .

It is possible to obtain some indication of the reasonableness of the computed Crampton result by noticing that the length of the thin wall tube does not enter into the formula. Consequently, after axial



slicing, and the  $D_1$  relaxation is noted, one can perform another cut, perpendicular to the cylinder axis, so two slit cylinders, each of length  $l/2$  can be obtained. These individual cylinders, can be examined concerning their new  $D_1$  values. If the new values differ considerably from the value produced by the first axial cut, then one can conclude that constant axial stress does not exist. The requirement that the stress varies linearly from inner wall to outer wall is illustrated in figure 1(b). Here, the shaded area represents the stress distribution according to the beam requirement. The sinusoidal type curve depicted therein might, however, be closer to the actual distribution. It is concluded that the use of slitting techniques provide, at best, a crude indication of the actual stress state in a given specimen. More accurate methods are described below.

### BLIND HOLE DRILLING METHODS

It should be noted that residual stresses cannot be measured directly. One must first determine the magnitude and algebraic sign of the strain that exists in a given sample under examination and then compute the residual stresses from the strain information. To obtain the strain information, the state of constraint of the material just beneath the strain gage is altered by removing a small amount of material adjacent to the gage. This is achieved by drilling a small hole in the center of a rosette, consisting of three linear gages (figure 2) bonded to the specimen and, connected to a digital strain indicator. The drilling operation relaxes the material at the edge of the hole, causes a local redistribution of the stress, which in-turn produces the strain change detected by the strain gages in the rosette.

It has been experimentally observed that the relaxed strains depend on the depth of the drilled hole. When the hole depth approximates the diameter, further drilling does not significantly change the strain gage readings; hence one normally takes as equilibrium surface strain values those obtained at a depth equal to the diameter of the drilled hole. Unless special precautions are taken when the hole is drilled, the strain gage readings will not only reflect the residual strains/stresses in the sample but will also reflect the strains produced by the hole drilling operation.

For a given state of stress, the strain gages sense relaxation signals which are proportional to the diameter of the drilled hole. It is desirable to obtain a strong signal by drilling a large hole. Care must be exercised, however, in selecting the drill size so that the cutting surface area is not too close to the gages and unduly perturb the true strain relaxation signal from the drilling operation. Holes of 0.159-cm (1/16-inch) diameter are normally used in practice, because

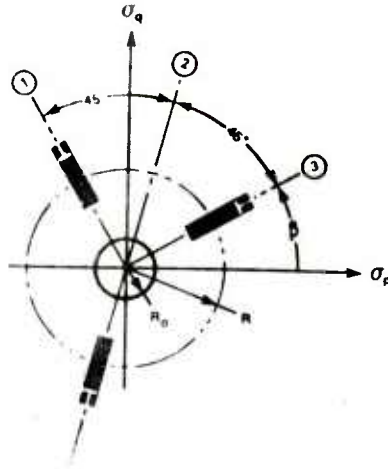


Figure 2. Relationship between the linear strain gage elements and the principal directions,

they provide relatively strong and unperturbed relaxation signals.

The radial distance from the center of the hole to the three linear elements in the rosette is critical because the strains are functions of the inverse second and inverse fourth powers of this radius. Therefore, one should use commercially available precision strain-gage rosettes and should not attempt to construct a homemade rosette by gluing down three linear gages because the formulas used to calculate the stress state assume that all three linear gages lie precisely on the same circle of radius  $R$ , and are symmetrically oriented with respect to each other; as shown in figure 2.

#### Hole Forming Methods

Various techniques have been described in the literature to produce the center hole in the strain gage rosette. These include the use of conventional drill bits, specially ground milling cutters, electric discharge machining, and abrasive jet machining.

Bush and Kromer (ref 3) have investigated some problems associated with the use of various methods to produce the center hole. Their results for annealed steel are shown in figure 3. It can be seen, for conventional drill bits, that unpredictable errors, ranging from  $60 \mu\epsilon$  to  $-70 \mu\epsilon$  can result. When these strain values are converted into stress, they amount to an error of  $\pm 124.11 \text{ MPa}$  ( $\pm 18 \text{ ksi}$ ). The rotating cutters cause an error ranging from  $-30 \mu\epsilon$  to  $-60 \mu\epsilon$ .

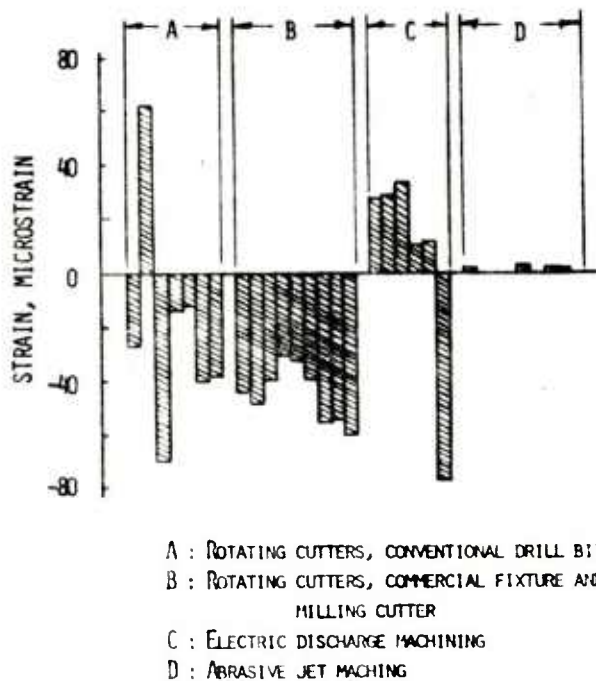


Figure 3. Strain effects caused by various hole producing methods.

The electric discharge machining can cause errors ranging from  $30 \mu\epsilon$  to  $-80 \mu\epsilon$ , depending on the hole diameter. The superiority of the abrasive jet machining method is obvious from the extremely low strain values of 2 or  $3 \mu\epsilon$  shown in figure 3. This method will be described in more detail later. For now, consideration will be given to the equations normally used to convert the measured strains into computed stresses.

The equations describing the principal stresses and their orientation with respect to the number three gage can be written in two different ways for the Blind Hole Method. This choice depends on whether or not one considers the linear gage element as a point gage (i.e., of infinitesimal length), or as one with a finite length, centered on the specimen, at the same location as the point gage. For the radially oriented point gage case, the principal stresses and their directions are given by (ref 4):

$$\sigma_p = \frac{\epsilon_3(A + B \cos 2\beta) - \epsilon_1(A - B \cos 2\beta)}{4AB \cos 2\beta}$$

$$\sigma_q = \frac{\epsilon_1(A + B \cos 2\beta) - \epsilon_3(A - B \cos 2\beta)}{4AB \cos 2\beta}$$

$$\beta = \frac{1}{2} \tan^{-1} \frac{(\epsilon_3 - 2\epsilon_2 + \epsilon_1)}{(\epsilon_3 - \epsilon_1)}$$

where

$$A = \frac{-(1 + \nu)}{2Er^2} \quad (2)$$

$$B = \frac{-(1 + \nu)}{2E} \left[ \left(1 - \frac{4}{r^2}\right) \frac{1}{r^2} - \frac{3}{r^4} \right]$$

$\epsilon_1$ ,  $\epsilon_2$ , and  $\epsilon_3$  are the measured strains,  $E$  and  $\nu$  are the elastic modulus and Poisson's ratio, respectively, and  $r$  is the ratio of the radius of the rosette to the radius of the drilled hole,  $R/R_0$ . The quantities  $\sigma_p$  and  $\sigma_q$  are the principal residual stress, while the angle  $\beta$  is measured to the number three gage element (fig. 2). When the equations listed above are used, it should be realized that the strain gages are assumed to act as point gages, i.e., of zero gage length. For the finite length gage, the equations for the principal stresses become (ref 5)

$$\sigma_{p,q} = E \left[ \frac{\epsilon_1 + \epsilon_3}{2S_1} + \frac{\epsilon_1 - \epsilon_3}{2S_2 \cos 2\beta_1} \right]$$

where

$$S_1 = (\nu - 1) + R_1 \text{ and } S_2 = -(\nu + 1) + R_2 \quad (3)$$

here

$$R_1 = \frac{1}{(r_2 - r_1)} \int_{r_1}^{r_2} r^2 \left(1 - \frac{a^2}{r^2}\right) - \nu \left(1 + \frac{a^2}{r^2}\right) dr$$

$$R_2 = \frac{1}{(r_2 - r_1)} \int_{r_1}^{r_2} \left( \left(1 - \frac{3a^4}{r^4} - \frac{4a^2}{r^2}\right) + \nu \left(1 + \frac{3a^4}{r^4}\right) \right) dr,$$

where  $r_1$  and  $r_2$  are the inner and outer edge dimensions of the active gage element, respectively, and  $a$  is the radius of the drilled hole.

An attempt was made to compare the difference in the computed stress value when both equation 2 and equation 3 were used with the same input strain data. The results are given in the table where it can be seen that the point gage equations (i.e., equations 2) produce numerical values for the residual stresses which are 10 to 20 percent higher than those produced by the finite length equations (i.e., equations 3).

#### Abrasive Jet Method

In this method, see figure 4, a carefully controlled stream of gas, containing 50  $\mu$  aluminum oxide powder, is directed against the workpiece in a manner which chips away microscopic particles of the material to drill the nominal 0.159-cm (1/16-inch) diameter hole.

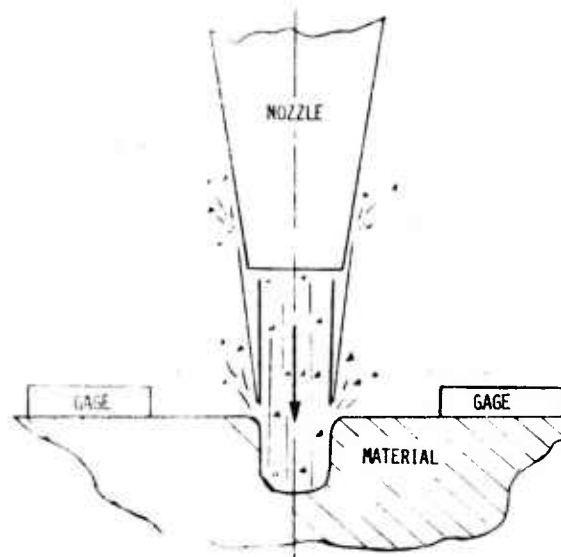


Figure 4. Experimental setup for abrasive jet machining.

Table. The effect of using point gage versus finite length gage equations in the computation of the residual stress

SAMPLE	ROSETTE	HOLE RADIUS  mm (inch)	STRAIN  μE	RESIDUAL STRESS USING BLIND HOLE METHOD						β Degree
				POINT GAGE COMPUTATION		FINITE LENGTH GAGE COMPUTATION				
				$\sigma_p$ MPa (KSI)	$\sigma_q$ MPa (KSI)	$\sigma_p$ MPa (KSI)	$\sigma_q$ MPa (KSI)	$\sigma_p$ MPa (KSI)	$\sigma_q$ MPa (KSI)	
1	A <sup>1</sup>	0.81(0.032)	472	509	447	-252.4(-36.6)	-273.7(-39.7)	-206.9(-30.0)	-226.2(-32.8)	38
	B <sup>1</sup>	0.81(0.032)	327	313	436	-218.6(-31.7)	-184.8(-26.8)	-196.5(-28.5)	-163.4(-23.7)	26
2	A <sup>1</sup>	0.86(0.034)	357	423	498	-219.3(-31.8)	-193.1(-28.0)	-199.3(-28.9)	-174.4(-25.3)	2
	B <sup>1</sup>	0.81(0.032)	378	323	462	-246.8(-35.8)	-204.8(-29.7)	-224.8(-32.6)	-183.4(-26.6)	33
3	A <sup>1</sup>	0.81(0.032)	346	382	254	-143.4(-20.8)	-180.0(-26.1)	-128.2(-18.6)	-164.8(-23.9)	28
	B <sup>2</sup>	0.81(0.032)	434	319	518	-220.6(-39.3)	-209.6(-30.4)	-248.2(-36.0)	-187.5(-27.2)	38

1. Hole was drilled by undercut end mill.

2. Hole produced by abrasive machining.



As seen in figure 3, the abrasive jet machining method appears to be the most gentle one to produce the central hole. Special precautions must be taken however to insure that the walls are relatively square with the surface on which the rosette is bonded. It is also desirable to insure that the hole is accurately positioned at the center of the rosette. For the cases where the hole is off-center, the iterative method proposed by Sandifer and Bowie (ref 6) can be used to obtain corrected values for the stress. When the hole is centered to within a few thousandths of an inch, the iterative method is not needed. Under certain circumstances, however, the formula used to compute the direction of the principal stress can be subject to large errors when small errors exist in the measured strain readings.

#### Indeterminacy of Beta

The quantities  $\epsilon_1$ ,  $\epsilon_2$ , and  $\epsilon_3$  are equal in an equal biaxial stress field. When these values are inserted into the expression for  $\beta$  in equation 2 they produce a value for  $\beta$  of 0 degrees. When  $\epsilon_1 = \epsilon_3 > \epsilon_2$  then  $\beta$  approaches +45 degrees. When  $\epsilon_1 = \epsilon_3 < \epsilon_2$ , then  $\beta$  approaches -45 degrees. In other words, slight errors in the measurement of  $\epsilon_2$  can produce large errors in the computed value for  $\beta$ . The two points to be emphasized are: (1) in an equal biaxial stress field the angle  $\beta$ , describing the principal stress directions, can fluctuate wildly; and (2) the algebraic sign and magnitude of the computed stress are not affected by this uncertainty in beta.

#### EFFECT OF THE CENTRAL HOLE ON THE MEASURED STRESS

It is well known from strain measurements and photoelastic experiments that geometrical discontinuities such as holes or notches act as stress raisers in plate material under tension. This multiplication of stress can be expressed in terms of a theoretical stress concentration factor  $K$ , given by the ratio of the maximum stress to the nominal stress on the net section. In other words,

$$K_t = \sigma_{\max} / \sigma_{\text{nominal}}$$

Both longitudinal and radial stresses are produced around a circular hole in material subjected to a load. When a uniaxial stress is present, and the hole is many diameters from the edge of the specimen, the radial, theta, and the shear components of stress are given by the Kirsch (ref 7) equations, namely:

$$\sigma_{rr} = \frac{\sigma}{2} \left( 1 - \frac{a^2}{r^2} \right) + \frac{\sigma}{2} \left( 1 + \frac{3a^4}{r^4} - \frac{4a^2}{r^2} \right) \cos 2\theta \quad (4)$$

$$\sigma_{\theta\theta} = \frac{\sigma}{2} \left(1 + \frac{a^2}{r^2}\right) - \frac{\sigma}{2} \left(1 + \frac{3a^4}{r^4}\right) \cos 2\theta$$

$$\tau_{r\theta} = -\frac{\sigma}{2} \left(1 - \frac{3a^4}{r^4} + \frac{2a^2}{r^2}\right) \sin 2\theta$$

Here,  $\sigma$  is the uniform applied tensile stress far removed from the hole. The quantity  $a$  is the hole radius, while  $r$  is the location where the  $r, \theta$  components of stress are desired. From the above equations, and inspection of figure 5, it can be seen that the maximum stress of  $3\sigma$  occurs at points C and A. Here,  $r = a$ , and  $\theta = 0^\circ$  and  $180^\circ$ . In other words,  $\sigma_{\theta\theta} = 3\sigma = \sigma_{\text{max}}$ . Hence,  $K_t = 3$ . It can also be seen that  $\sigma_{\theta\theta} = -\sigma$  at points D and B when  $r = a$  and  $\theta = 90^\circ$  and  $270^\circ$ , respectively. Hence, a tensile stress, far removed from the hole, produces at points B and D, a compressive stress of equal magnitude.

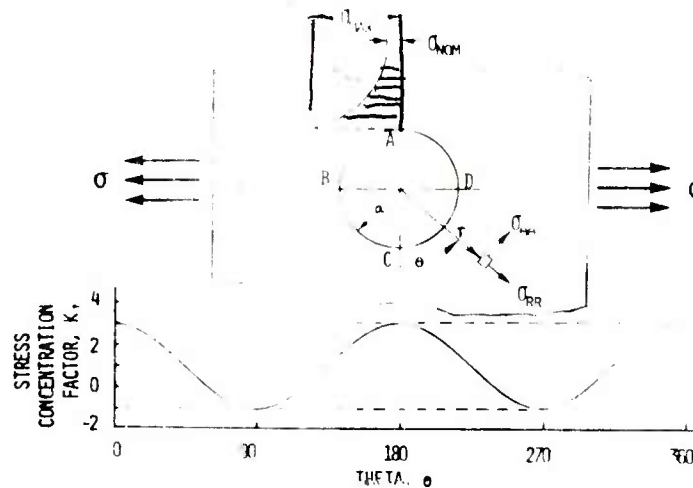


Figure 5. Effect of the stress concentration factor on the state of stress in a uniaxially stressed plate.



The net effect of the stress concentration factor is to produce plasticity at the edge of the drilled hole when the measured stress exceeds one-third of the yield stress for cases where the gages are positioned in a uniaxial field. When the gage is positioned in an equal biaxial field, plasticity occurs when the measured stress exceeds one-half of the yield stress. Beaney and Procter (ref 8) have shown, for the uniaxial case, that at stress values less than half yield, the errors are negligible while at full yield, the errors can rise to 10 percent.

#### X-ray Measurement of Stress

In brief, the X-ray method measures the shift of the diffracted beam when the sample surface is rotated a known amount in the incident beam. From the measured peak shift one computes the change in the lattice spacing and attributes the shift to residual macrostresses. In other words, the interplanar spacing change is used as a strain gage indicator to compute the biaxial stress residing on the outer surface of the sample. The mathematics describing the X-ray method is adequately described in section 2 of an SAE booklet (ref 9). Equation 31 of Section 2 in (ref 9) shows that the stress is given by

$$\sigma = \frac{E}{(1 + \nu)} \frac{1}{\sin^2 \psi} \frac{\cot \theta}{2} \frac{\pi}{180} (2\theta_1 - 2\theta\psi) \quad (5)$$

where

E is the modulus of elasticity

$\nu$  is Poisson's ratio

$\psi$  is the angle the sample normal was rotated in the X-ray beam

$\theta$  is the angle of incidence of the X-ray beam with the atomic planes

$2\theta$  is the angular position of the diffracted X-ray beam when the sample bisects the incident and diffracted X-ray beams

$2\theta\psi$  is the position of the diffracted X-ray beam when the sample is rotated an additional  $\psi$  degrees about a vertical axis lying in the plane of the sample and perpendicular to the plane of the incident and diffracted X-ray beams

There is some controversy in the literature concerning the appropriate values to use for Young's modulus and Poisson's ratio; however, the SAE paper (ref 9) gives a technique in Section 6.4 for experimentally

determining these quantities.

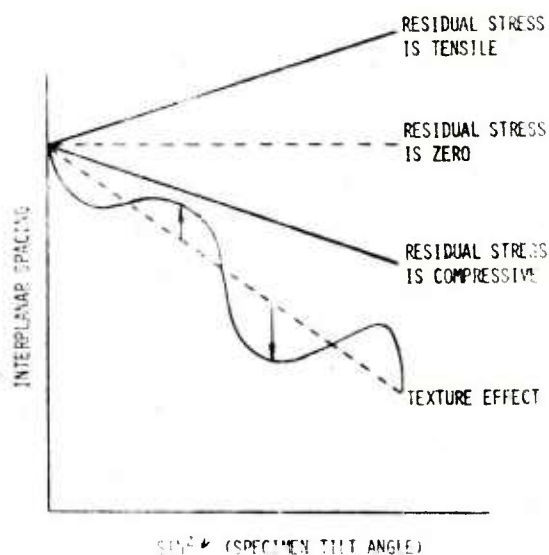


Figure 6. Interplanar spacing plot for different residual stress states.

Equation 5 implies that the interplanar spacing,  $d$ , is linearly dependent on  $\sin^2\psi$ . From figure 6 it can be seen that a positive slope is produced by a tensile stress, a negative slope by a compressive stress, and a slope of zero by a residual stress of zero. For highly textured samples, the interplanar spacing values oscillate above a least square line drawn through the experimental data points. It is found, experimentally, that the curve is above the mean straight line for those orientations where the reflecting pole density is higher than the random level and below it where it is lower than the random level. It is believed that the larger-than-expected values for the interplanar spacing results from stress relaxation by dynamic recovery.

To understand these findings, the shape of the modified stress-strain curve shown in figure 7 and proposed by Cullity (refs 10 and 11), and Smith and Wood (ref 12) should be evaluated. It should be noted that the positive abscissa describes the contraction of the  $(hkl)$  spacing when the stress direction is at right angles to the normal of the diffracting grains. Curve A-B-C, the total strain curve, consists of an elastic portion, A-B, and an elastic-plastic portion, B-C. In the elastic region, the strain measured by X-rays, called the lattice strain, and that measured by mechanical methods (i.e., total strain) are both proportional to the applied stress, and have the same slope.

In other words, the lattice strain curve and the mechanically measured total strain curve are superimposed on each other along the path A-B. In addition, both curves return to zero when the applied stress is removed if the material has not been taken into the yield region. When the applied stresses exceed the elastic limit, the X-ray method presupposes that the lattice strain follows the line B-D. In practice, however, it deviates significantly from the line B-D and follows the curve B-E. As the applied stress is released the lattice strain curve follows the path E-F, and has the same slope as the path A-B.

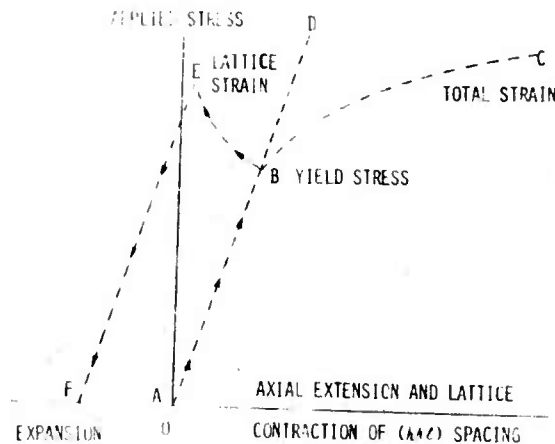


Figure 7. Lattice and total stress-strain curve.

Thus, this result will produce a net mean compressive residual lattice strain which is represented by F-A, with large fluctuations from the mean being exhibited by individual diffracting crystallinities. This net residual lattice strain produces an observed X-ray line shift which is interpreted by the X-ray stress formula as an indication of the presence of compressive macrostrain in the specimen. The picture becomes clearer when one considers the findings of other researchers (refs 13, 14, and 15) and also remembers that the X-ray diffraction signal arises predominantly from coherently diffracting domains which are centered in the subgrain interior regions.

Cullity proposes a rather new explanation for the anomalous computed residual stress values for uniaxially plastically elongated materials. He cites the work of Keh and Weissman (ref 16), Neurath and Waite (ref 17), and Morrill (ref 18) which indicate that, in uniaxially elongated metals, the subgrain walls remain in tension. Because the

X-ray beam predominately samples the subgrain interior, it can readily be seen that equation 5 is preconditioned to predict overall compressive stresses in the sample. The reverse prediction would occur if the subgrains were put into tension, by uniaxial compression.

Marion and Cohen (ref 2) have extended the work of Weidemann (ref 9) and have put forth the formula given below to describe the behavior of the interplanar spacing  $d_{\phi,\psi}$  on  $\sin^2\psi$ . Here the nonlinear dependence of  $d$  on  $\sin^2\psi$  is attributed to the relief of microstrains in subgrain interiors. The degree of relief depends on the orientation of the grain to the stressing system and to the texture developed during the plastic deformation process. The Marion-Cohen approach separates the nonlinear and linear components of  $d$  by means of the expression

$$d_{\phi,\psi} = (d_{\max} - d_B) f(\alpha,\beta) + d_{\perp} \frac{(1 + \nu)}{E} \sigma_{\phi} \sin^2\psi + d_B \quad (6)$$

The term  $d_{\max}$  is the interplanar spacing in a region where the strain is fully relieved, while  $d_B$  corresponds to a region which has not been relieved. This means that the quantity  $(d_{\max} - d_B)$  describes the range of interplanar spacings present in the sample. The distribution function  $f(\alpha,\beta)$ , describes the orientation dependence of  $d$  and is obtained from the observed integrated intensity of the diffraction peak at each  $\psi$  inclination. The distribution function is normalized to unity. Equation 6 is solved by measuring the interplanar spacing,  $d_{\phi,\psi}$ , and the normalized distribution function,  $f(\alpha,\beta)$ , as a function of  $\sin^2\psi$  for six orientations of the sample. This overdetermined system of equations is solved by means of a least squares computation to yield the stress,  $\sigma_{\phi}$ . The necessity of using equation 6 for a given sample is readily determined by plotting interplanar spacing measurements as a function of  $\sin^2\psi$  for 5 or 6 orientations of the sample. If the plot is linear, then the standard formula shown in equation 5 can be used to compute the stress. When the plot oscillates, the more sophisticated Marion-Cohen expression must be used.

#### SUMMARY

It can be shown that the indiscriminate use of dissection strain gage and X-ray methods to determine the stress state of specimens can introduce large errors in the computed result.

Note that for thin-walled tubes that the Crampton dissection method required a condition of plain strain in addition to a linear variation of the stress from the inside wall surface to the outside wall surface. Since the formula to compute the maximum circumferential stress was length independent, the condition of plain strain could be readily

verified by cutting the slit tube, of length  $\ell$  into two tubes of length  $\ell/2$  whereby the new diameters could be compared with the diameter obtained from the slit tube of length  $\ell$ .

A comparison of various blind-hole drilling methods in annealed steel indicated that abrasive jet machining causes a negligible error in contrast to other hole drilling methods which introduce errors range from +60 to -70  $\mu\epsilon$ . It was pointed out that the standard equations to convert strain readings to computed stresses assume that the strain gage is in reality a point gage (i.e., one of zero length). When the actual gage length is taken into account, the computed stresses can vary significantly. For cases where the strain gage is placed in an equal biaxial stress field, it was shown that small errors in the measurement of  $\epsilon_2$  can produce large fluctuations in the computed value for  $\beta$ .

The standard X-ray stress equations were reviewed, and it was noted that a nonlinear plot of interplanar spacing versus  $\sin^2 \psi$  identified those samples where the standard X-ray equations could not be used. The oscillating dependence of  $d$  on  $\sin^2 \psi$  was attributed to the relief of microstrains during extensive plastic deformation and the production of a strong texture. The curve tended to lie above a mean straight line drawn through the data points for diffracting plane orientations where the pole density was higher than the random level and below it where it was lower than the random level. When measurements of the interplanar spacing were taken for six  $\psi$  tilts, the non-linear dependence of  $d$  could be separated from the linear component by using the Marion-Cohen formula.

#### REFERENCES

1. B. D. Cullity, "Some Problems in X-ray Stress Measurements," Advances in X-ray Analysis, Vol 20, Plenum Press, New York, (1977), pp 259-271.
2. R. H. Marion and J. B. Cohen, "Anomalies in Measurement of Residual Stress by X-ray Diffraction," Advances in X-ray Analysis Vol. 18, Plenum Press, New York, (1974), pp. 466-501.
3. A. J. Bush and F. J. Kromer, "Simplification of the Hole-Drilling Method of Residual Stress Measurement," ISA Transactions, Vol 12, No. 3, (1973), pp 249-259.
4. "Measurements of Residual Stresses by the Blind Hole Drilling Method," Technical Data Bulletin T-403, (1977), Photolastic Inc.



5. K. P. Milbradt, "Ring-Method Determination of Residual Stresses," Proc. Soc. Exptl. Stress Anal., Vol. 9, No. 1, (1951), pp 63-74.
6. J. P. Sandifer and G. E. Bowie, "Residual Stress by Blind-Hole Method with Off-Center Hole," Exp. Mech., 18, No. 5, (May 1978), pp 173-179.
7. G. Kirsch, "Die Theorie der Elastizitat und die Bedürfnisse der Festigkeitslehre," Zeitschrift des Vereines Deutscher Ingenieure, Vol. 42, (July 16, 1898), pp 797-807.
8. E. M. Beaney and E. Procter, "A Critical Evaluation of the Centre Hole Technique for the Measurement of Residual Stresses," Strain, (Jan. 1974), pp 7-14, 52.
9. M. E. Hilley, J. A. Larson, C. F. Jataczak, and R. E. Ricklefs, eds. "Residual Stress Measurements by X-ray Diffraction," SAE Report J 784a (1971), Available from SAE, Inc., 400 Commonwealth Drive, Warrendale, PA 15096.
10. B. D. Cullity, "Residual Stress After Plastic Elongation and Magnetic Losses in Silicon Steel," Trans. Met. Soc., Vol. 227, (1963), pp 356-358.
11. B. D. Cullity, "Sources of Error in X-ray Measurements of Residual Stress," JAP35, (1964), pp 1915-1917.
12. S. I. Smith and W. A. Wood, "Internal Stress Created by Plastic Flow in Mild Steel, and Stress-Strain Curves for the Atomic Lattice of Higher Carbon Steels," Proc. Royal Society, Series A 182, (1944) pp 404-415.
13. G. B. Greenough, "Residual Lattice Strains in Plastically Deformed Metals," Nature 160, (1947), p 258.
14. G. B. Greenough, "Residual Lattice Strains in Plastically Deformed Polycrystalline Metal Aggregates," Proc. Royal Society, Series A, 197, (1949), pp 556-567.
15. M. J. Donachie and J. T. Norton, "Lattice Strains and X-ray Stress Measurement," Trans Met. Society, AIME 221, (1961), pp 962-967.
16. L. S. Darken, "Some Observations on Atoms and Imperfections," Trans. Quarterly Amer. Society Metals, 54, (1961), pp 559-642, (fig. 30 by Keh and Weissman).

17. P. W. Neurath and R. E. Waite, "Elastic and Plastic Strains and Watt Losses in Grain-Oriented Three PCT Si-Fe," Trans. AIME 203, (1955), p 480.
18. W. Morrill, "Silicon Irons up to Date," Metals Progress 78, (1960), pp 84-87.
19. W. Wiedemann Ph. D., Thesis, "Technische Hochschule," Aachen, Germany, (1966).

## DISTRIBUTION LIST

Director  
Defense Research and Engineering Office  
ATTN: DDRE (R&AT) Mr. J. Persh  
Washington, DC 20310

Director  
Defense Advanced Research Projects Agency  
ATTN: Dr. E. Van Redth  
1400 Wilson Blvd  
Arlington, VA 22209

Defense Technical Information  
ATTN: Accessions Divisions (DDC-TC) (12)  
Cameron Station  
Alexandria, VA 22314

Assistant Secretary of the Army (R&D)  
ATTN: Deputy for Science and Technology  
Washington, DC 20310

Deputy Chief of Staff for Research,  
Development and Acquisition  
Department of the Army  
ATTN: DAMA-ARZ-D  
Washington, DC 20310

Commander  
U.S. Army Materiel Development and Readiness Command  
ATTN: DRCMT, L. Croan  
DRCMD-D  
DRCMD-DT  
DRCMD-R  
DRCDE-DE  
DRCDE-E, Mr. E. Gardner  
DRCDE-I  
DRCDE-W  
Technical Information Division  
5001 Eisenhower Avenue  
Alexandria, VA 22333



Commander

U.S. Army Armament Research and Development Command

ATTN: DRDAR-CG, MG A. H. Light Jr.  
DRDAR-TD, Dr. R.E. Weigle  
DRDAR-TDR, Dr. R. J. Eichelberger  
DRDAR-SC, Col. M. G. Swindler  
DRDAR-SC, Dr. D. Gyorog  
DRDAR-SCM, Mr. J. D. Corrie  
DRDAR-SCM-P, Dr. E. Bloore  
DRDAR-SCM-M, Mr. W. Dittrich  
DRDAR-SCM-P, Dr. J. Waldman  
Mr. J. Beetle  
Mr. J. Mulherin  
Mr. I. G. Betz  
Mr. F. Witt (10)  
Mr. F. M. Lee  
Mr. W. Rider  
Mr. P. Miller  
Mr. J. Rinnovatore  
DRDAR-LC, Col. D. P. Whalen  
DRDAR-LCU, Mr. B. Bushey  
Mr. B. Gustad  
Mr. W. Sharp  
Mr. D. Robertson  
DRDAR-LCU-SS, Mr. R. Botticelli  
Mr. W. Field  
DRDAR-TS, Col. D. E. Wright  
DRDAR-TSS (5)  
DRDAR-QA, Mr. D.G. Adams  
DRDAR-QAR-I, Mr. M. Weinberg  
DRDAR-QAR-Q, Mr. R. Blakeslee  
Mr. F. Cohen  
DRDAR-SCP  
DRCPM-CAWS, Col. R. R. Phillipp  
DRCPM-SA, Col. C. Jones, Jr.  
DRCPM-ADG, Col. L. Marrella  
DRCPM-PBM, Col. H. V. Dutchyshyn  
DRCPM-NUC  
DRCPM-AAH (30 mm)  
DRCPM-TMA  
DRDAR-LCA-G, Mr. I. Rosendorf  
Mr. G. Bubb  
Dr. S. Yim

Dover, NJ 07801

Commander

U. S. Army Research Office

ATTN: Director, Metallurgy & Materials Science Division

PO Box 12211

Research Triangle Park, NC 27709

Commander  
U. S. Army Materials and Mechanics Research Center  
ATTN: DRXMR, Dr. E. Wright  
DRXMR-PT  
AMXMR-EQ, Dr. C. Gazzara  
DRXMR-MQ, Mr. W. Roy  
Technical Information Division  
Watertown, MA 02172

Commander  
Naval Air Development Center, Johnsville  
Warminster, PA 18974

Aero Materials Department  
ATTN: Mr. F. Williams, Man  
Dr. W. S. Scott, Man  
Warminster, PA 18974

Commander  
U. S. Naval Engineering Experimental Station  
ATTN: Materials Lab. WCTRL-2  
Annapolis, MD 21401

Director  
U. S. Army Mobility Equipment Research and Development Command  
ATTN: DRDME-MMM, E. York  
Fort Belvoir, VA 22060

Commander  
U.S. Army Research and Standardization Group (Europe)  
ATTN: DRXSN-E-RM, Dr. R. Quattrone  
PO Box 65  
FPO, New York 04510

Commander  
U.S. Naval Surface Weapons Center  
ATTN: W. Mannschreck, Code G54  
Dahlgren, VA 22448

Commander  
Naval Surface Weapons Center  
White Oak Laboratory  
ATTN: A. P. Divecha, M/S R-32  
Silver Spring, MD 20910

Commander  
U.S. Army Aviation Materiel Command  
ATTN: Technical Information Division  
P.O. Box 209, Main Office  
St. Louis, MO 63166

Commander  
U.S. Army Communications and Electronics Materiel Readiness Command  
ATTN: Technical Information Division  
Fort Monmouth, NJ 07703

Commander  
Rocky Mountain Arsenal  
ATTN: Technical Information Division  
Denver, CO 80240

Commander  
U.S. Army Research Office  
ATTN: Metallurgy & Materials Science Division,  
G. Mayer, Director  
PO Box 12211  
Research Triangle Park, NC 27709

Commander  
Redstone Scientific Information Center  
ATTN: DRDMI-T-B-D, Bldg 4484  
Redstone Arsenal, AL 35809

Commander  
U.S. Army Foreign Science & Technology Center  
ATTN: Mr. W. F. Marley  
220 Seventh Street, N.E.  
Charlottesville, VA 22901

Director, Ames Directorate  
U.S. Army Air Mobility R&D Lab  
ATTN: SAVDL-AM  
Ames Research Center  
Moffett Field, CA 94035

Director, Langley Directorate  
U.S. Army Air Mobility R&D Lab  
ATTN: SAVDL-LA, M/S 266  
B. Lisagor, M/S 188B  
Hampton, VA 23365

Director, Lewis Directorate  
U.S. Army Air Mobility R&D Lab  
ATTN: SAVDL-LE  
21000 Brook Park Road  
Cleveland, OH 44135

Director, ARRADCOM  
USA Ballistic Research Laboratories  
ATTN: Dr. A. M. Dietrich, DRDAR-BLT  
Dr. S. Golaski, DRDAR-BLT  
Mrs. P. W. Kingman, DRDAR-BLT  
Mr. J. Simon, DRDAR-BLT  
Technical Library, DRDAR-TSB-S  
Technical Library, DRDAR-CLJ-L  
Aberdeen Proving Ground  
Aberdeen, MD 21005

Benet Weapons Laboratory  
Technical Library  
ATTN: DRDAR-LCB-TL  
Watervliet, NY 12189

Commander  
U.S. Army Armament Materiel Readiness Command  
ATTN: DRSAR-LEP-L  
Rock Island, IL 61299

Director  
U.S. Army TRADOC Systems Analysis Activity  
ATTN: ATAA-SL (Technical Library)  
White Sands Missile Range, NM 88002

U.S. Army Materiel Systems Analysis Activity  
ATTN: DRXSY-MP  
Aberdeen Proving Ground, MD 21005

Librarian  
National Bureau of Standards  
Washington, DC 20025

National Academy of Science  
Materials Advisory Board  
ATTN: Dr. J. R. Lane  
2101 Constitution Ave., N.W.  
Washington, DC 20418

Metals & Ceramics Information Center  
Battelle Memorial Institute  
505 King Avenue  
Columbus, OH 43201

U.S. Atomic Energy Commission  
Document Library  
Germantown, MD 21403

Commander  
Aeronautical Systems Division  
ATTN: Technical Library  
Director, Air Force Materials Laboratory  
Wright Patterson AFB  
Dayton, OH 45433

National Aeronautics & Space Administration  
Federal Bldg #10  
ATTN: Code RRM  
Washington, DC 20456

Drexel University  
Materials Engineering Dept.  
ATTN: Prof. A. Lawley  
Philadelphia, PA 19104

Bethlehem Steel Corp.  
Homer Research Labs  
ATTN: Dr. E. Kottecamp  
Bethlehem, PA 18018

Dr. Paul Flynn  
215 Tuscany Drive  
Baltimore, MD 21210

Weapon System Concept Team/CSL  
ATTN: DRDAR-ACW  
Aberdeen Proving Ground, MD 21010

Technical Library  
ATTN: DRDAR-CLJ-L  
Aberdeen Proving Ground, MD 21010

Director  
U.S. Army Ballistic Research Laboratory  
ARRADCOM  
ATTN: DRDAR-TSB-S (STINFO)  
Aberdeen Proving Ground, MD 21005

Commander  
U.S. Army Armament Materiel Readiness Command  
ATTN: DRSAR-LEP-L  
Rock Island, IL 61299